CHEMISTRY
A EUROPEAN JOURNAL

DOI: 10.1002/chem.200902196

Structural Diversity in the Self-Assembly of Pseudopeptidic Macrocycles

Ignacio Alfonso,*[a] Miriam Bru,[b] M. Isabel Burguete,[b] Eduardo García-Verdugo,[b, c] and Santiago V. Luis*[b]

Abstract: The self-assembling abilities of several pseudopeptidic macrocycles have been thoroughly studied both in the solid (SEM, TEM, FTIR) and in solution (NMR, UV, CD, FTIR) states. Detailed microscopy revealed large differences in the morphology of the self-assembling micro/nanostructures depending on the macrocyclic chemical structures. Self-assembly was triggered by the presence of additional methylene groups or by changing from *para* to *meta* geometry of the aromatic phenylene backbone moiety. More interestingly, the nature of the side chain also plays a fundamental role in some of the obtained nanostructures, thus producing structures from long fibers to hollow spheres. These nanostructures were obtained in different solvents and on different surfaces, thus implying that the chemical information for the self-assembly is contained in the molecular structure. Dilution NMR studies (chemical shift and self-diffusion rates) suggest the formation of incipient aggregates in solution by a combination of hydrogen-bonding and π–π interactions, thus implicating amide and aryl groups, respectively. Electronic spectroscopy further supports the π–π interactions because the compounds that lead to fibers show large hypochromic shifts in the UV spectra. Moreover, the fiber-forming macrocycles also showed a more intense CD signature. The hydrogen-bonding interactions within the nanostructures were also characterized by attenuated total-reflectance FTIR spectroscopy, which allowed us to monitor the complete transition from the solution to the dried nanostructure. Overall, we concluded that the self-assembly of this family of pseudopeptidic macrocycles is dictated by a synergic action of hydrogen-bonding and π–π interactions. The feasibility and geometrical disposition of these interactions finally render a hierarchical organization, which has been rationalized with a proposal of a model. The understanding of the process at the molecular level has allowed us to prepare hybrid soft materials.

Keywords: macrocycles · nanostructures · pseudopeptides · self-assembly · supramolecular chemistry

Introduction

The preparation and study of new hierarchically self-assembled organic materials is one of the most interesting research topics in supramolecular chemistry.[1] The controlled formation of supramolecular entities within the micro/nanometric scale from simple and accessible building blocks is of enormous importance for technological[2] and biomedical applications.[3] Among all the possible building blocks, those based on peptidic moieties are especially attractive, as they allow a large structural diversity through side-chain replacements.[4] In addition, they usually show good biocompatibility and chemical stability, thus making them highly interesting for biotechnological applications.[5] Recently, very elegant designs inspired by nature have been described. Thus, cage-like structures,[6] amphyphilic molecules,[7] and helical[8] or β-sheet[9] sequences have been used as starting templates for further modification and development. However, the complete understanding of the aggregation process remains

[a] Dr. I. Alfonso
Departamento de Química Biológica y Modelización Molecular
Instituto de Química Avanzada de Cataluña
Consejo Superior de Investigaciones Científicas (IQAC-CSIC)
Jordi Girona, 18-26, 08034, Barcelona (Spain)
Fax: (+34) 932-045-904
E-mail: ignacio.alfonso@iqac.csic.es

[b] Dr. M. Bru, Dr. M. I. Burguete, Dr. E. García-Verdugo, Prof. Dr. S. V. Luis
Departamento de Química Inorgánica y Orgánica
UAMOA, Universidad Jaume I/CSIC
Campus del Riu Sec, Avenida Sos Baynat
s/n, 12071, Castellón (Spain)
Fax: (+34) 964-728-214
E-mail: luiss@qio.uji.es

[c] Dr. E. García-Verdugo
Current address: Instituto de Catálisis y Petroleoquímica
CSIC, Campus de la UAM
C/Marie Curie,2 Cantoblanco, Madrid 28049 (Spain)

Supporting information for this article is available on the WWW under http://dx.doi.org/10.1002/chem.200902196.

elusive because very small structural changes can lead to strikingly different sizes and shapes of the self-assembled nanostructures.[10] Therefore, for the bottom-up construction of peptide-like self-assemblies, deep knowledge of the implicated intermolecular interactions is mandatory. Unfortunately, that information has not been always possible to extract from experimental data. With this aim, the availability of a wide family of relatively simple compounds with systematic structural modifications should be desirable.

In regard to that aim, we recently reported versatile synthetic methodologies for the preparation of large-size pseudopeptidic macrocycles by changing many different structural variables in a modular fashion.[11] On the other hand, smaller related compounds efficiently self-assemble in different organic solvents, thus leading to the formation of supramolecular gels.[12] Accordingly, we selected some representative pseudopeptidic macrocycles (Scheme 1) to study their

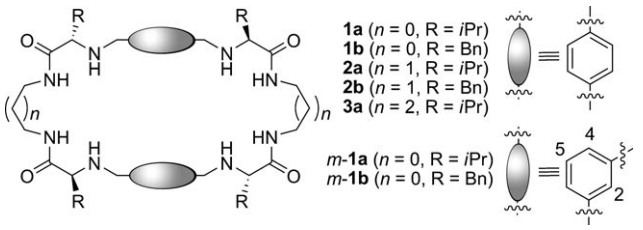

Scheme 1. Chemical structure of pseudopeptidic macrocycles.

self-assembly behavior by using different techniques both in the solid (SEM, TEM, FTIR) and solution (NMR, UV, CD, FTIR) states. More importantly, the transition from the solution to the nanostructure was monitored in situ by attenuated total reflectance FTIR (ATR-FTIR) for the first time. The compounds were selected for mapping the effects of several structural variables, such as the aromatic backbone (*para*/*meta*) geometry, the aliphatic spacer ($n=0$, 1), or the nature of the amino acid side chain (aliphatic/aromatic). This study allowed us to obtain very valuable information on the self-assembly process, which led us to the preparation of hierarchical hybrid nanostructures.

Results and Discussion

Study of the morphology of the solid-state self-assembled nanostructures: We used SEM for visualization of self-assembled structures on the micro/nanometric scale. Samples were prepared by dissolving 2–3 mg of the corresponding compounds in chloroform containing a small amount of methanol (typically 5–10% MeOH, approximately 1–2 mg mL^{-1} final concentration of macrocycle). These solutions were carefully added onto the SEM sample holder (aluminum) and slowly evaporated at room temperature. The SEM images of the dry residues of some selected examples are shown in Figures 1–3. The corresponding *para* derivatives with the shortest spacer ($n=0$; **1a**,**b**) did not show any detectable nano-/microstructure, thus leading to amorphous materials upon drying (see Figures S1 and S2 in the Supporting Information). However, increasing the aliphatic spacer between the peptidic moieties ($n=1$, 2) had an important impact on the SEM images. Compound **2a** derived from valine (Figure 1a) showed the formation of small

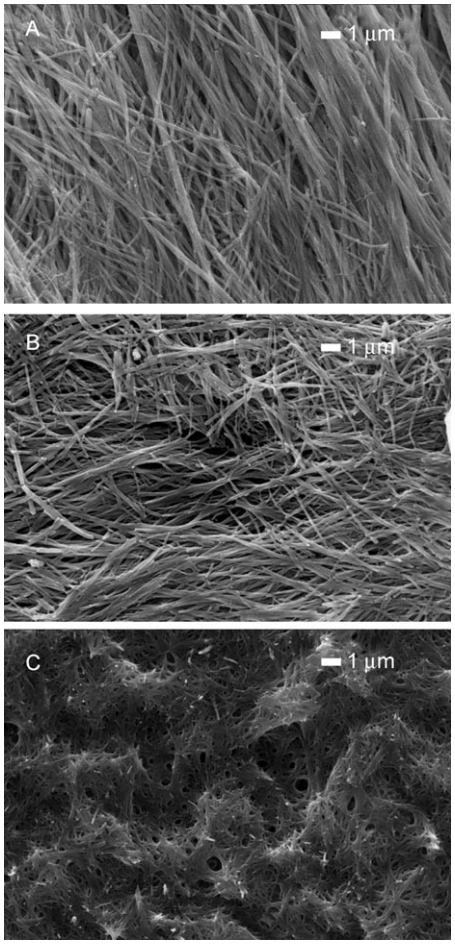

Figure 1. SEM images of a) **2a**, b) **3a**, and c) **2b** grown from $CHCl_3$/MeOH (9:1) on an aluminum surface.

fibers (length: ca. 20 μm, width: ca. 160 nm). Very similar microstructures were obtained with additional methylene groups in the aliphatic spacers for **3a** ($n=2$; Figure 1b). On the other hand, the phenylalanine counterpart of **2a** (**2b**, $n=1$; Figure 1c) also showed the formation of self-assembled fibrils of similar width (~150 nm) but were significantly shorter (1–3 μm). In addition, they form an interpenetrated network that left curved spaces between the fibrils (Figure 1c). Interestingly, the *meta* derivative *m*-**1a** (R = *i*Pr, $n=0$) self-assembled into straight fibers (Figure 2a). These fibers are long (50–150 μm) with a width of about 500 nm (Figure 2b). They uniformly covered the whole surface of the holder and showed a more regular distribution than those from **2b** or **3a**. Similar, though slightly smaller, fibrilar suprastructures of *m*-**1a** were also obtained by using different solvents (e.g., CH_3CN/MeOH 3:1; Figure 2c) or on top

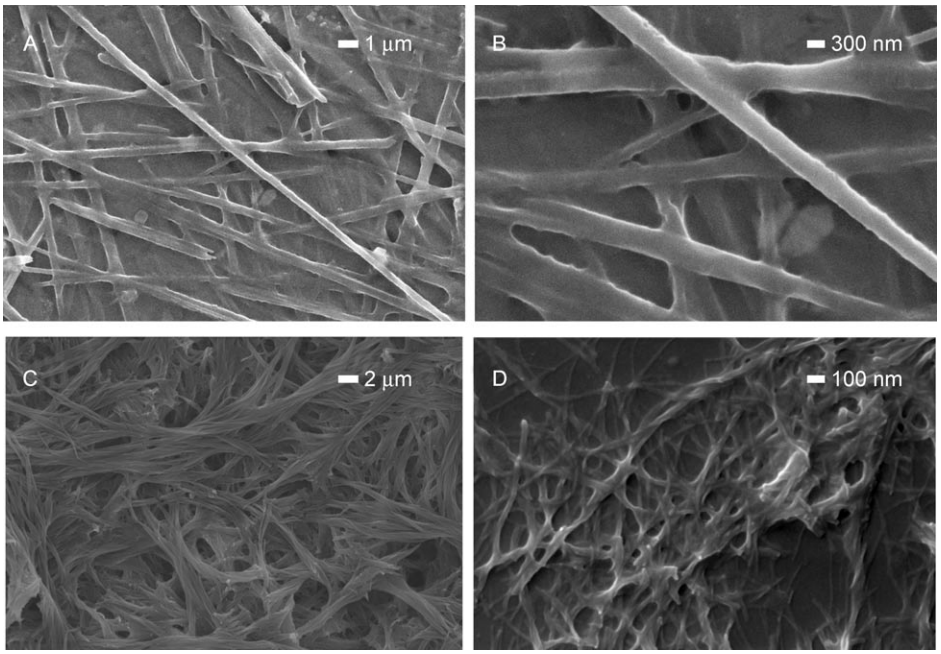

Figure 2. SEM images of *m*-**1a** grown from a, b) $CHCl_3$/MeOH (9:1) dried onto an aluminum surface, c) CH_3CN/MeOH (3:1) dried onto an aluminum surface, and d) $CHCl_3$/MeOH (9:1) dried onto a glass surface.

of a different surface (e.g., glass; Figure 2d). These experiments suggest that the self-assembly process is effective in different environments, such as solvent composition and/or surface nature.

Surprisingly, when the side chains of the peptidic moieties were replaced by benzyl groups in the *meta* derivative (*m*-**1b**), spherical structures with a diameter of approximately 0.5–3 μm were obtained (Figure 3a, b). These spheres were reproducible in shape and size on different surfaces (aluminum, glass, mica, or holey carbon; see Figure 3c and Figures S4–S6 in the Supporting Information) or from several solvents (CH_3CN/MeOH 3:1; Figure 3d), and they were not accompanied with other morphologies, such as small fibrils or tapes.[10a] A detailed inspection of the SEM images showed the presence of a hole in some of these spheres (Figure 3b, d), most likely due to the rapid evaporation of the contained solvent during vacuum metalation for SEM analysis.[13] This behavior suggests that the spherical structures have a hollow vesicular nature, which was further confirmed by TEM analysis (Figure 3c). Overall, the microscopy showed the influence of different structural parameters on the self-assembly abilities of the pseudopeptidic macrocycles. Thus, completely different morphologies and sizes were obtained by simple and controlled structural changes in the macrocyclic building block. In addition, the experiments carried out with different solvents and on different surfaces suggest that the self-assembly is dictated by the chemical information contained in the molecular structures, with only small effects from external factors.

NMR solution studies: The intriguing behavior of the self-assembly of these pseudopeptidic macrocycles led us to study their structure in solution to further detect the key intermolecular interactions that lead to the final self-assembled nanostructures. All the compounds studied herein showed an averaged D_2 symmetry on the NMR timescale, which suggests a relatively high flexibility of the macrocyclic rings in solution. However, some of them showed a concentration dependence of the chemical shifts of representative signals. Thus, for instance, when in-

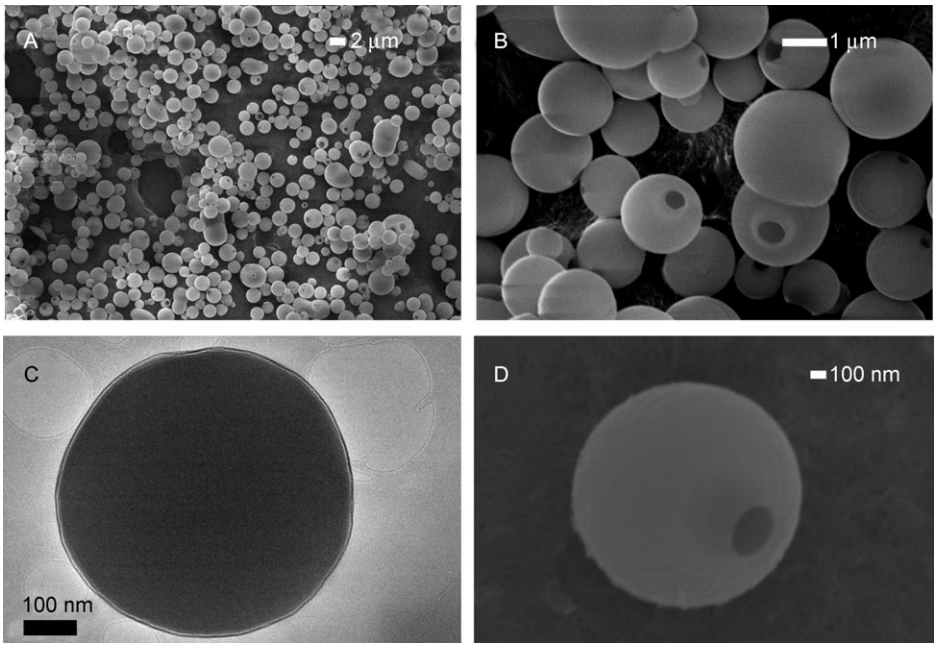

Figure 3. a, b) SEM images of *m*-**1b** grown from $CHCl_3$/MeOH (9:1) dried onto an aluminum surface; c) TEM image of *m*-**1b** grown from a $CHCl_3$/MeOH (9:1) onto a holey carbon copper grid; d) SEM image of *m*-**1b** grown from a CH_3CN/MeOH (3:1) dried onto an aluminum surface.

creasing the global concentration of *m*-**1a** from 0.41 to 41.0 mM, the corresponding ^{1}H NMR spectra showed a downfield shift of the amide NH proton signal ($\Delta\delta =$ 0.18 ppm) and an upfield shift ($\Delta\delta = -0.05$–0.08 ppm) of the protons from the *m*-phenylene moiety (Figure 4a,b). The signs of the chemical shift $\Delta\delta$ suggest the existence of intermolecular hydrogen-bonding and π–π stacking interactions, thus implicating amide and aromatic groups, respectively.[14] Within all the concentration range studied herein, we observed a single set of signals, thus implying a fast exchange regime on the NMR timescale (Figure 4a) for the self-assembly process as well. The nonlinear fitting of the chemical shift of the NH proton signal to an isodesmic self-aggregation model[15] (see Figure S8 in the Supporting Information) rendered an association constant of $K = 35.7 \pm 9.8\ \text{M}^{-1}$.[16] The self-diffusion rate of *m*-**1a** was also measured by DOSY experiments at different overall concentrations.[17] The apparent *D* value, measured with the methyl protons of the *i*Pr group, decreased from $D = 6.35 \pm 0.10 \times 10^{-10}\ \text{m}^2\text{s}^{-1}$ at 1.6 mM to $D = 5.43 \pm 0.06 \times 10^{-10}\ \text{m}^2\text{s}^{-1}$ at 32.0 mM. These changes would imply an increase of approximately 60% in the average volume of the species in solution, and an apparent aggregation number of 5–8 within this concentration range (see Table S1 in the Supporting Information). All these NMR spectroscopic data strongly support the formation of incipient self-assembled nanostructures in solution.

We performed similar experiments with *m*-**1b**, which self-assembled into spherical nanostructures (Figure 4c). In this case, we also observed a downfield shift of the amide NH proton and upfield shifts of the aromatic protons. However, the significantly smaller downfield shift of the amide protons ($\Delta\delta = 0.10$ ppm) suggests a lower participation of hydrogen bonding in the intermolecular interactions. On the other hand, the concentration-dependent shielding of the protons of the benzylic side chains ($\Delta\delta = -0.04$–0.05 ppm) were slightly larger than those for the *m*-phenylene moiety ($\Delta\delta = -0.03$–0.04 ppm), thus highlighting the main importance of the π–π stacking of the aromatic side chains in the self-assembly process of *m*-**1b**. Additionally, the isodesmic model fitting of the NH signal yielded weaker binding (i.e., $K = 9.6 \pm 2.3\ \text{M}^{-1}$; see Figure S8 in the Supporting Information). The moderate binding constants obtained herein must be considered taking into account that a mixture of competitive solvents for both hydrogen-bonding (methanol) and hydrophobic (chloroform) interactions were used for the experiments. Furthermore, similar dilution experiments performed with the corresponding *para* derivatives (**1a**,**b**) produced very small changes in the ^{1}H NMR spectra (see Figures S9 and S10 in the Supporting Information), thus suggesting a much weaker intermolecular interaction.[18]

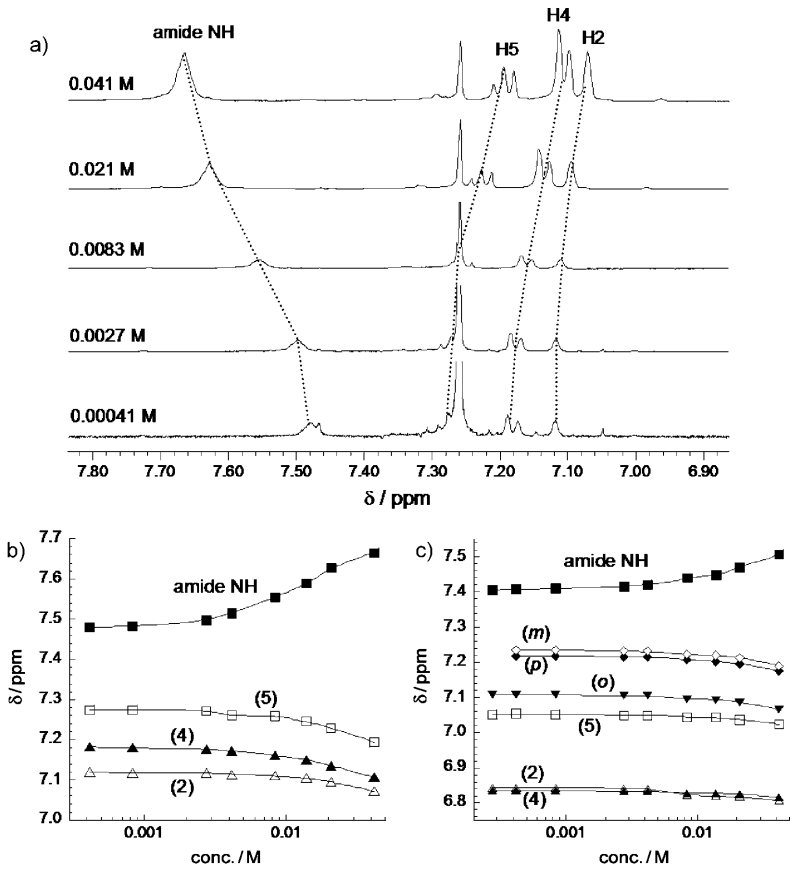

Figure 4. a) Selected partial ^{1}H NMR spectra of *m*-**1a** (500 MHz, 30 °C, $CDCl_3$/MeOH 9:1) at different overall concentrations. Plot of the concentration (log scale) dependence of ^{1}H NMR spectroscopic data of b) *m*-**1a** and c) *m*-**1b** (both at 500 MHz, 303 K). Arbitrary atom numbering of the *m*-phenylene moiety is shown in Scheme 1, whereas *ortho* (*o*), *meta* (*m*), and *para* (*p*) refers to the positions on the aromatic side chains of *m*-**1b**.

Electronic absorbance and CD spectroscopy: The self-assembly process in solution was additionally studied by absorbance and CD electronic spectroscopy. Compound **1a** showed an UV spectrum with two almost equally intense bands at $\lambda = 240$ and 260 nm due to the aromatic phenylene electronic transitions (Figure 5a, gray). The spectrum of *m*-**1a** showed a large hypochromic shift, especially in the band at $\lambda = 260$ nm (Figure 5a, black). This lower absorbance is not related to the different aromatic-ring substitution because the other *para*-derivatives **2a** and **3a** yielded a very similar spectrum (Figure 5a, dashed black and dashed gray for **2a** and **3a**, respectively). Interestingly, SEM images had shown the formation of fibrils

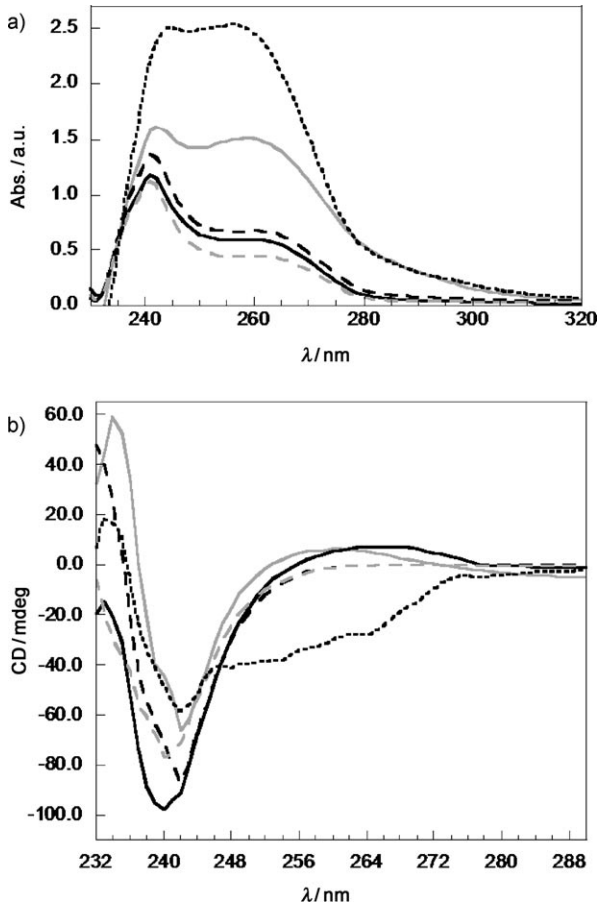

Figure 5. a) UV and b) CD spectra (0.85 mM, $CHCl_3$/MeOH 95:5) of **1a** (gray), *m*-**1a** (black), **2a** (dashed), **3a** (dashed gray), and *m*-**1b** (dotted).

for *m*-**1a**, **2a**, and **3a**, but not for **1a**. Therefore, there is a direct relationship between the hypochromic shift in the UV spectra and the self-assembly trends. A similar hypochromic shift had been previously observed in aromatic self-assembled systems and was ascribed to establishing π– π stacking interactions.[19] The CD spectra of these derivatives were also informative (Figure 5b). The negative cotton effect at $\lambda = 240$ nm was larger for the macrocycles that showed fibril formation (*m*-**1a**, **2a**, and **3a**) than for **1a**. This behavior is consistent with a decreased conformational freedom within the self-assembled supramolecular structure and is also in agreement with reported data in other fiber-forming chiral systems.[20] On the other hand, the CD spectra of *m*-**1b** (forming self-assembled spherical structures) showed a less intense negative Cotton effect at $\lambda = 240$ nm. The additional CD signal at $\lambda = 250$–260 nm could be assigned to the disposition of the aromatic side chains in a chiral environment. It is difficult to directly compare *m*-**1a** and *m*-**1b**, as the latter has a much more intense UV spectrum. However, the somehow lower relative CD signal of *m*-**1b** can be related to the sphere formation.[20,21]

ATR-FTIR vibrational spectroscopy: Vibrational spectroscopy has several singularities that make it especially useful for studying these self-assembly processes. First, because the frequency range for vibrations has a very different value, fast processes on the NMR timescale can be accessible and differentiable by using IR spectroscopic analysis. On the other hand, IR spectroscopy can be easily performed on virtually any state of matter. Thus, we performed ATR-FTIR measurements with slowly evaporated samples of *m*-**1a** (fibers) and *m*-**1b** (spheres), whereas **1a** was used as the control (Table 1). Several types of C=O bands were observed for **1a**, thus showing β-sheet, random, and turn conformations.[22] In addition, the high amide A frequency at 3400 cm^{-1} implies little hydrogen-bonding aggregation, thus explaining the absence of self-assembling structures in SEM analysis. For *m*-**1b**, we also observed the presence of different carbonyl conformations, although the amide A band suggests some degree of hydrogen bonding. Therefore, we can hypothesize the partial participation of hydrogen bonding in the formation of the microspheres of *m*-**1b**. On the other hand, a strongly hydrogen-bonded carbonyl group was observed upon the formation of the fibers with *m*-**1a**. The values of the vibrational frequencies correspond to the formation of β-sheet/β-stack-type aggregation motifs.[23] The observation of only one carbonyl type for the fibers of *m*-**1a** suggests that the molecule shows a highly symmetrical conformation within the self-assembled fiber. Remarkably, ATR-FTIR measurements were performed on a ZnSe surface, which again indicate that the self-assembly processes do not rely on the nature of the surface.

Table 1. ATR-FTIR data (cm^{-1}) of **1a** and *m*-**1a-b** obtained from slowly evaporated samples.

Compound	Amide I	Amide II	Amide A
1a	1636, 1646, 1652	1507–1559	3400, 3306
m-**1a**	1636	1553, 1541	3278
m-**1b**	1636, 1650, 1655	1523, 1548	3289

We further attempted to obtain a more precise image of the complete process that leads from the self-assembled structures in solution to the nano-/microstructures in the solid state. With this aim, we prepared samples of *m*-**1a**,**b** (40 mM in $CHCl_3$/MeOH 9:1) and studied the time dependence of the FTIR spectra during the slow evaporation of the solvent onto an ATR sample holder (Figure 6). The key bands (amide A, I and II) for selected spectra were deconvoluted into the corresponding vibrational peaks (see Figures S11–S16 in the Supporting Information). Thus, for instance, the amide A band was decomposed into the vibrations that correspond to associated NH and free NH groups (< 3300 and 3400 cm^{-1}, respectively). In both cases, the slow evaporation of the solvent was accompanied with an increase in the hydrogen-bonded associated peak. This transition was practically complete for *m*-**1a** (see Figure 6a and Figure S11 in the Supporting Information), whereas for *m*-**1b** (see Figure 6b and Figure S14 in the Supporting Information) a considerable amount of non-hydrogen-bonded NH protons were still present in the dried sample. This find-

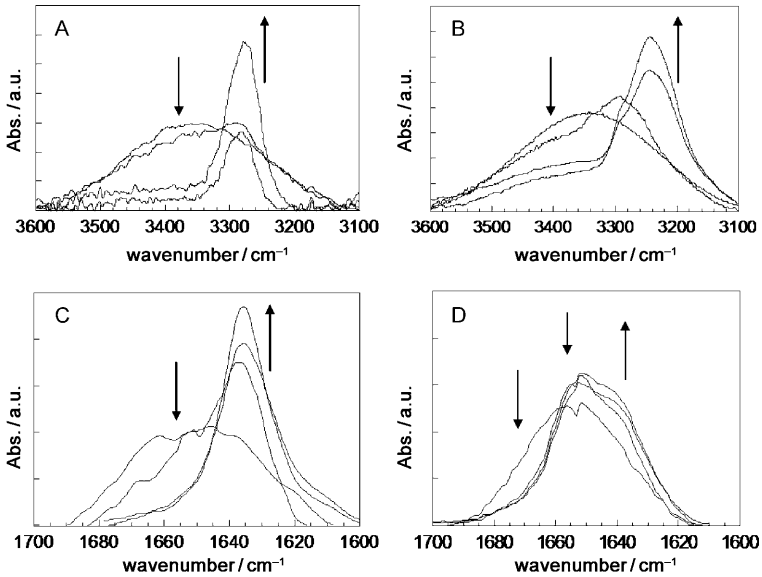

Figure 6. Solvent evaporation evolution for selected sections of the ATR-FTIR spectra of A) amide A for *m*-**1a**, B) amide A for *m*-**1b**, C) amide I for *m*-**1a**, and D) amide I for *m*-**1b**.

ing suggests that the intermolecular hydrogen bonds are more important for the formation of the fibers than for the formation of the spheres. The deconvolution of amide I bands was also very informative. The FTIR spectrum of *m*-**1a** in solution showed the presence of a β-stack (1636 cm^{-1}) and turn or random (1650–1670 cm^{-1}) conformations (see Figure 6c and Figure S12 in the Supporting Information). During the drying process, the proportion of the β-stack structures increased up to being practically exclusive within the fibers of *m*-**1a**. These observations imply that the dynamic flexible structure present in solution (several carbonyl groups) undergoes a conformational transition to a more rigid and symmetrical conformation (only one carbonyl group) within the solid aggregates. On the other hand, the same study with *m*-**1b** showed the presence of β sheets accompanied with turn conformations during all the drying process (see Figure 6d and Figure S15 in the Supporting Information). Parallel results were obtained by comparing the corresponding amide II bands in *m*-**1a**,**b** (see Figures S13 and S16 in the Supporting Information). Thus, we can conclude that different types of amide groups are present in the final spherical self-assembly due to either intramolecular folding of the molecule or the coexistence of different conformations.[24]

Molecular modeling: We also performed molecular-modeling calculations on the isolated macrocycles **1a**, **2a**, *m*-**1a**, and *m*-**1b** to visualize the conformational effects produced in the macrocyclic core by the different structural variables. The three-dimensional disposition of the different functional groups must define the feasibility and geometry of the potential intermolecular interactions (hydrogen bonding, π–π, hydrophobic). According to our experimental results, the noncovalent intermolecular contacts ultimately dictate the self-assembly process. Thus, the conformational analysis of the macrocycles could shed some light onto the different behavior for the formation of the corresponding nano-/microstructures. A stochastic conformational search was applied without restrictions to each compound (a Monte Carlo search followed by a Merck molecular force-field (MMFF) minimization; Figure 7A–D). The theoretical data suggest that **1a** with the short spacer ($n=0$) and *para* substitution (Figure 7A) tends to set the aromatic rings perpendicular to the macrocyclic main plane,[11a,b,e] thus avoiding the possibility of establishing intermolecular aromatic–aromatic in-

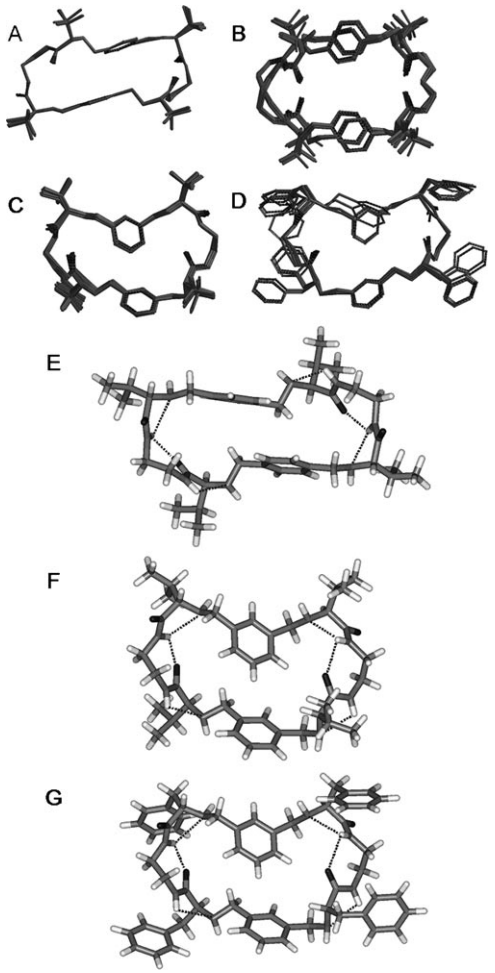

Figure 7. Upper view of the superposition of the energetically accessible local minima for A) **1a**, B) **2a**, C) *m*-**1a**, and D) *m*-**1b**. The global minima for E) **1a**, F) *m*-**1a**, and G) *m*-**1b** are shown with possible intramolecular hydrogen bonds in dashed lines.

teractions in a stacked-ring self-aggregation model (see below). However, increasing the aliphatic spacer (**2a**; Figure 7B, $n=1$) or changing the substitution of the aromatic phenylene ring from *para* to *meta* (*m*-**1a**; Figure 7C) changes the relative disposition of the aromatic rings and sets them nearly in the same plane of the macrocyclic ring. Therefore, we hypothesize that in these systems (i.e., **2a** and *m*-**1a**) there is the possibility of establishing aromatic stacking interactions in the direction perpendicular to the macrocyclic ring.[12b] In the case of *m*-**1b**, the Monte Carlo analysis rendered similar results to *m*-**1a**, although a slightly more flexible ring was found (Figure 7D). Furthermore, in this case, the aromatic side chains tend to fold over the amide bonds, thus protecting them from forming intermolecular hydrogen bonds.[25] For a better visualization of the hydrogen-bonding pattern that implicates amide NH protons, the global minima for **1a**, *m*-**1a**, and *m*-**1b** are shown in Figure 7E–G, respectively. In all the cases, they form intramolecularly hydrogen-bonded turns, as expected for isolated systems of this type. In solution, we experimentally observed a clear D_2 symmetry of the ^{1}H and ^{13}C NMR signals,[11b] which means that the optimized geometries must be in fast equilibrium with the complementary ones to finally render the observed average molecular symmetry. On the other hand, these structures are in very good agreement with the solution FTIR spectral data, which showed the presence of turn conformations for all the tested compounds. As the timescale for both spectroscopic techniques is very different, the experimental observations are consistent with the theoretical conformational analysis: the fluxionality of the macrocycles seems to be fast on the NMR timescale but slow on the IR timescale.

Proposal of a self-assembling mechanism: Taking into account all the experimental and theoretical results, we propose a reasonable model for the observed self-assembly processes. All the compounds show a fluxional conformation in solution by NMR spectroscopic analysis. The molecular-modeling studies suggest that they tend to form intramolecular hydrogen-bonded turns, which is consistent with the FTIR spectral data in solution. Thus, we can propose a conformational equilibrium as depicted in Scheme 2 for *m*-**1a**, in which complementary intramolecularly hydrogen-bound conformers (**I** and **II**) are in equilibrium with the fully symmetric flat conformation (**III**). The interconversion of the species (**I**–**III**) would explain both the observed average symmetry by NMR spectroscopic analysis and the different carbonyl groups detected by using solution FTIR spectroscopy. The symmetrical conformer **III** allows synergic establishment of intermolecular hydrogen-bonding (detected by ^{1}H NMR and FTIR) and π–π (detected by ^{1}H NMR and UV) interactions, thus leading to its aggregation. Within this model, the two interactions responsible for the assembly would take place at both faces of the ring and in the same direction, namely, perpendicular to the macrocyclic plane. The consecutive self-association along this preferred direction, followed by packing of the tubes thus-formed would

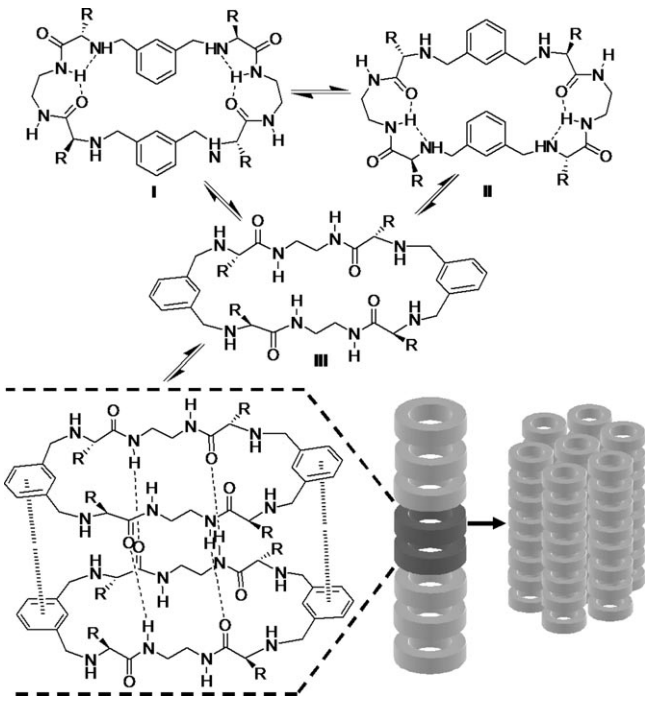

Scheme 2. Proposed model for the self-assembly of *m*-**1a**.

eventually produce the growth of fibers (Scheme 2). The molecules of *m*-**1a** within these fibers must show only one type of carbonyl group with a β-sheet/β-stack vibrational frequency, exactly as experimentally observed for the dried fibers of *m*-**1a**. Therefore, this model explains the observation of fibers by SEM analysis and is consistent with the experimental data obtained in solution for *m*-**1a** (NMR, UV, FTIR) and the transition from a flexible conformation to a β-stacked structure, as observed by using ATR-FTIR spectroscopy to monitor the drying process.

This model also allowed us to explain the observed differences between the other derivatives. For the formation of the fiber, both hydrogen bonding and π–π stacking must take place in the direction of the growth. The short *para* derivatives (**1a** and **1b**) tend to set the aromatic phenylene unit perpendicular to the macrocyclic main ring (Figure 7A,D for **1a**), thus precluding the proposed π–π interactions and disfavoring the self-assembly. This behavior is consistent with the SEM, NMR, UV, and FTIR spectroscopic data of **1a**. However, increasing the aliphatic spacer with *para* derivatives (**2a** and **3a**) favors the setting of the aromatic rings in the macrocyclic main plane, as shown by molecular modeling (Figure 7B). Once again, this disposition would allow the establishment of π–π interactions at both faces of the macrocycle and perpendicular to it. The stacking of the aromatic rings agrees with the hypochromic shift in the UV spectra of **2a** and **3a**. Thus, this model also explains the formation of fibers in derivatives bearing longer aliphatic spacers ($n=1$, 2). The particular case of the spheres obtained with *m*-**1b** is a bit more difficult to rationalize. The molecular modeling data suggests that the aromatic side chain could shield the amide NH groups from in-

termolecular interactions.[25] This behavior would imply that conformers I and II (Scheme 2) would prevail in solution, as detected by FTIR spectroscopic analysis. Under those circumstances, self-assembly is mainly dictated by the π–π interactions of the side chains (as suggested by NMR), which must be less directional and finally produces spherical self-assembled microstructures. Within these spheres, different carbonyl conformations would be present (structures **I** and **II** in Scheme 2), in good agreement with the FTIR spectroscopic data of dried samples of *m*-**1b**.

Hierarchical self-assembly for the construction of hybrid mixed nanostructures: We also studied the ability of the systems to self-aggregate hierarchically into hybrid microstructures.[26] We focused on the *meta* derivatives *m*-**1a**,**b**, which led to fibers or hollow spheres. We prepared equimolecular solutions of *m*-**1a**+*m*-**1b** ($CHCl_3$/MeOH 9:1) and the obtained mixture was added onto the SEM holder then slowly dried. The SEM micrographs showed the formation of homogeneous spherical microstructures (Figure 8A–D). These

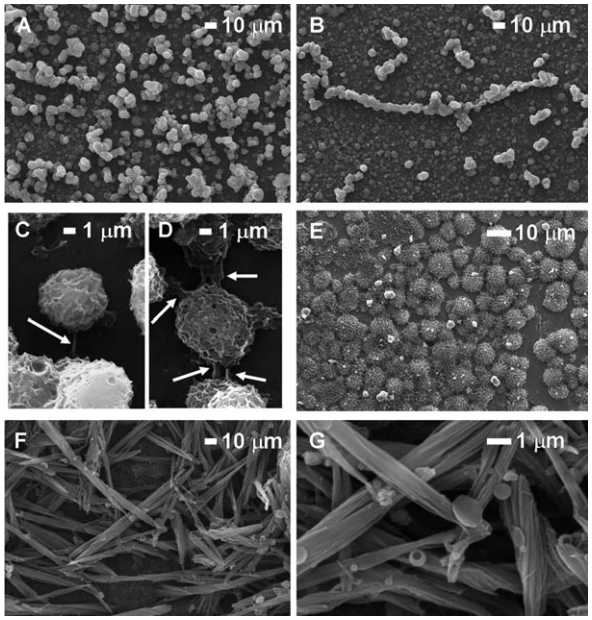

Figure 8. A,B) SEM images of a mixture of solutions of *m*-**1a** and *m*-**1b** in $CHCl_3$/MeOH (9:1). C,D) Magnified sections of (A) and (B). E) Sample obtained by the consecutive addition of solutions of 1) *m*-**1a** and 2) *m*-**1b** in $CHCl_3$/MeOH 9:1. F,G) SEM images of a mixture of *m*-**1a** and *m*-**1b** grown from CH_3CN/MeOH (3:1). All the samples were grown onto aluminum surfaces.

spheres are grouped in bunches (Figure 8A) or connected in necklace-like microstructures (Figure 8B). This observation suggested that the surface of the spheres was covered by a fibril-like material that interpenetrates to render the observed junctions. A more careful inspection of the microstructures supported that hypothesis (the connecting fibrils are marked with arrows in Figure 8C,D).

An explanation for these results could be that the formation of the spheres of *m*-**1b** occurs faster, then the molecules of *m*-**1a** deposit and self-assemble on the surface of the preformed spheres of *m*-**1b**. We also obtained similar results by sequentially adding *m*-**1a** and *m*-**1b**, thus leading to hairy spherical morphologies, most likely produced by the coverage of the vesicles of *m*-**1b** with fibrils of *m*-**1a** (Figure 8E). These experiments confirmed the proposal of different rates of formation of both microstructures. The slower growth of the fibers of *m*-**1a** can be rationalized from the microscopic point of view: the self-assembly of the macrocycles into straight fibers requires a conformational transition, as observed by monitoring the process with ATR-FTIR spectroscopic analysis. Considering our hypothesis, the growth of the spheres must be slowed down to get self-discrimination of separated fibers and vesicles. We could slow down the growth by performing the experiments in CH_3CN/MeOH (3:1) as the solvent. As this mixture evaporates more slowly than the previous, the macrocycles were able to hierarchically self-organize to segregate into straight fibers and hollow vesicles (Figure 8F,G), with a very similar morphology to the structures obtained from pure samples of either *m*-**1a** or *m*-**1b**.

Conclusions

Herein, we have used the combination of different spectroscopic techniques (NMR, UV/CD, FTIR) to obtain fundamental information on the forces that direct the self-assembly of this family of pseudopeptidic macrocycles, thus leading to the formation of different nano-/microstructures, as observed by microscopy. Thus, the self-assembly process was triggered either by the presence of additional methylene groups in the aliphatic spacers or by the change from *para* to *meta* substitution of the aromatic backbone. Even more interestingly, the nature of the amino acid side chain can determine the morphology of the obtained nanostructure from long fibers to spherical vesicles. In addition, the self-assembly seems to be weakly dependent on external factors, such as solvent composition or surface nature. Therefore, the obtained nano-/microstructure must be a supramolecular expression of the chemical information stored in the molecular structures.

Studies using different techniques (NMR, UV, CD, ATR-FTIR) support the incipient self-assembly in solution through the cooperative action of hydrogen bonding and π–π stacking interactions. The combination of the strength and geometrical disposition of those contacts finally leads to different nanostructures. Additionally, we could monitor the structural changes that accompany the formation of the different nanostructures by following the drying process by ATR-FTIR spectroscopic analysis. We observed the formation of fibers for systems that allow the cooperative formation of amide hydrogen-bonding and aromatic π–π stacking interactions, both in the same direction, namely, perpendicular to the macrocyclic ring. For this disposition, the amide

bond plane has to be aligned with the fibril axis, whereas the aromatic ring should be set perpendicular to that direction and thus parallel to the macrocyclic main plane. The particular case of vesicle formation has also been rationalized by the structural/conformational characteristics of the chemical structure of the macrocyclic building block. Overall, this family of macrocycles displayed a widely diverse self-assembly behavior, which helped us to understand the molecular basis of the supramolecular process. We envision that our study will help to further design and prepare similar systems that could show interesting potential applications in bionanotechnology.

Experimental Section

General: Reagents and solvents were purchased from commercial suppliers (Adrich, Fluka, or Merck) and were used without further purification. Compounds **1a**,**b**, **2a**,**b**, **3a**, and *m*-**1a**,**b** were prepared as previously described.[11b]

Electron microscopy: SEM was performed either on a LEO 440I or in a JEOL 7001F microscope with a digital camera. Samples were obtained by slow evaporation of a solution of the macrocycles (ca. 1–2 $mg\,mL^{-1}$ either in $CHCl_3/CH_3OH$ 9:1 or CH_3CN/CH_3OH 3:1) directly onto the sample holder and were conventionally coated prior to the measurement. TEM was carried out on a JEOL 2100 microscope at 120 kV. The micrographs of *m*-**1b** were obtained from solutions of approximately 1 $mg\,mL^{-1}$ in $CHCl_3$/MeOH 9:1 on a holey carbon copper grid. The samples were sonicated for 10 min prior to the measurement and one drop was added onto the grid then collected directly without staining.

NMR spectroscopy: The NMR spectroscopic experiments were carried out on a Varian INOVA 500 spectrometer (500 and 125 MHz for ^1H and ^{13}C NMR, respectively). The chemical shifts are reported in ppm using trimethylsilane (TMS) as a reference. For the diffusion measurements, the standard DgcsteSL (DOSY Gradient Compensated Stimulated Echo with Spin Lock) sequence was used. The diffusion parameters were optimized for every sample to obtain 90–95% on signal intensity decay. An array of 15–30 values of gradient strength was acquired with 32–128 scans per value (depending on the sample concentration). The data were processed with the DOSY macro available in the Varian software. For the quantitative measurements, the isopropyl methyl signals were used to obtain the best signal-to-noise ratio. We used TMS (10 mM) as an internal standard in all the samples to check that the viscosity of the medium remained constant for all the samples and equal to the pure solvent mixture ($CDCl_3/CD_3OD$ 9:1). The measurements were repeated at least three times, thus yielding equal *D* values within the experimental error.

IR spectroscopy: FTIR spectra were acquired on a JASCO 6200 equipment with a MIRacle single-reflection ATR diamond/ZnSe accessory. We prepared a sample of the corresponding macrocycle (40 mM, $CHCl_3/CH_3OH$ 9:1) and we seeded it onto the ATR sample holder. We sequentially collected the FTIR spectra until complete solvent evaporation was reached. The raw IR spectral data were processed with the JASCO spectral manager software, and the deconvolution of the bands was performed with the Origin software using Gaussian-shaped ideal peaks.

UV and CD spectroscopy: Spectra were recorded with on a JASCO J-810 spectropolarimeter at room temperature.

Molecular modeling: All the theoretical calculations were performed using the Spartan '06 program. The optimized geometries for the corresponding minima were obtained as follows: A stochastic conformational search was applied (a Monte Carlo Search followed by MMFF minimization) without restrictions to each compound. A complete number of 10000 conformers were generated and at least 100 conformers were selected with an energy cut-off point of 10 $kcal\,mol^{-1}$. The obtained structures were ordered by their energies and analyzed. The Boltzmann distribution at 298 K and the molecular volume of *m*-**1a** were also calculated with Spartan '06. The superposition of the energetically accessible local minima was carried out by using the same software package.

Acknowledgements

This work was supported by the Spanish Ministerio de Ciencia e Innovación (CTQ2009-14366-C02) and CSIC-I3 (200780I001). M.B. also thanks the MEC for personal financial support (FPU).

[1] a) P. Pramod, K. G. Thomas, M. V. George, *Chem. Asian J.* **2009**, *4*, 806–823; b) J. M. Lehn, *Science* **2002**, *295*, 2400–2403; c) G. M. Whitesides, B. Grybowsky, *Science* **2002**, *295*, 2418–2421.

[2] a) Y. B. Lim, M. Lee, *J. Mater. Chem.* **2008**, *18*, 723–727; b) N. Ashkenasy, W. S. Horne, M. R. Ghadiri, *Small* **2006**, *2*, 99–102; c) W. S. Horne, N. Ashkenasy, M. R. Ghadiri, *Chem. Eur. J.* **2005**, *11*, 1137–1144; d) M. Reches, E. Gazit, *Science* **2003**, *300*, 625–627.

[3] a) T. D. Sargeant, M. S. Rao, C. Y. Koh, S. I. Stupp, *Biomaterials* **2008**, *29*, 1085–1098; b) Y. Chau, Y. Luo, A. C. Y. Cheung, Y. Nagai, S. Zhang, J. B. Kobler, S. M. Zeitels, R. Langer, *Biomaterials* **2008**, *29*, 1713–1719; c) R. Langer, D. A. Tirrell, *Nature* **2004**, *428*, 487–492; d) J. D. Hartgerink, E. Beniash, S. I. Stupp, *Proc. Natl. Acad. Sci. USA* **2002**, *99*, 5133–5138.

[4] a) I. Cherny, E. Gazit, *Angew. Chem.* **2008**, *120*, 4128–4136; *Angew. Chem. Int. Ed.* **2008**, *47*, 4062–4069; b) R. V. Ulijn, A. M. Smith, *Chem. Soc. Rev.* **2008**, *37*, 664–675; c) E. Gazit, *Chem. Soc. Rev.* **2007**, *36*, 1263–1269.

[5] S. Fernández-Lopez, H. S. Kim, E. C. Choi, M. Delgado, J. R. Granja, A. Khasanov, K. Kraehenbuehl, G. Long, D. A. Weinberger, K. M. Wilcoxen, M. R. Ghadiri, *Nature* **2001**, *412*, 452–455.

[6] a) S. Ghosh, S. K. Singh, S. Verma, *Chem. Commun.* **2007**, 2296–2298; b) S. Ghosh, M. Reches, E. Gazit, S. Verma, *Angew. Chem.* **2007**, *119*, 2048–2050; *Angew. Chem. Int. Ed.* **2007**, *46*, 2002–2004.

[7] a) L. C. Palmer, S. I. Stupp, *Acc. Chem. Res.* **2008**, *41*, 1674–1684; b) T. Rehm, V. Stepanenko, X. Zhang, F. Würthner, F. Gröhn, K. Klein, C. Schmuck, *Org. Lett.* **2008**, *10*, 1469–1472; c) C. Schmuck, T. Rehn, K. Klein, F. Gröhn, *Angew. Chem.* **2007**, *119*, 1723–1727; *Angew. Chem. Int. Ed.* **2007**, *46*, 1693–1697; d) S. J. Yang, S. Zhang, *Supramol. Chem.* **2006**, *18*, 389–396; e) T. Koga, M. Higuchi, T. Kinoshita, N. Higashi, *Chem. Eur. J.* **2006**, *12*, 1360–1367; f) S. Ye, B. M. Discher, J. Strzalka, T. Xu, S. P. Wu, D. Noy, I. Kuzmenko, T. Gog, M. J. Therien, P. L. Dutton, J. K. Blasie, *Nano Lett.* **2005**, *5*, 1658–1667; g) J. D. Hartgerink, E. Beniash, S. I. Stupp, *Science* **2001**, *294*, 1684–1688; h) T. C. Holmes, S. De Lacalle, X. Su, G. Liu, A. Rich, S. Zhang, *Proc. Natl. Acad. Sci. USA* **2000**, *97*, 6728–6733.

[8] a) W. C. Pomerantz, V. M. Yuwono, C. L. Pizzey, J. D. Hartgerink, N. L. Abbot, S. H. Gellman *Angew. Chem.* **2008**, *120, 1261–1264; Angew. Chem. Int. Ed.* **2008**, 47, 1241–1244; *Angew. Chem. Int. Ed.* **2008**, *47*, 1241–1244; b) W. Cai, G.-T. Wang, Y.-X. Xu, X.-K. Jiang, Z.-T. Li, *J. Am. Chem. Soc.* **2008**, *130*, 6936–6937; c) H. Dong, S. E. Paramonov, J. D. Hartgerink, *J. Am. Chem. Soc.* **2008**, *130*, 13691–13695; d) F. Rúa, S. Boussert, T. Parella, I. Díez-Pérez, V. Branchadell, E. Giralt, R. M. Ortuño, *Org. Lett.* **2007**, *9*, 3643–3645; e) T. A. Martinek, A. Hetényi, L. Fülöp, I. M. Mády, G. K. Tóth, I. Dékány, F. Fülöp, *Angew. Chem.* **2006**, *118*, 2456–2460; *Angew. Chem. Int. Ed.* **2006**, *45*, 2396–2400; f) M. Crisma, C. Toniolo, S. Royo, A. I. Jiménez, C. Cativiela, *Org. Lett.* **2006**, *8*, 6091–6094.

[9] a) A. Angelici, G. Falini, H.-J. Hofmann, D. Huster, M. Monari, C. Tomasini, *Angew. Chem.* **2008**, *120*, 8195–8198; *Angew. Chem. Int. Ed.* **2008**, *47*, 8075–8078; b) S. Hanessian, V. Vinci, K. Fettis, T. Maris, M. T. P. Viet, *J. Org. Chem.* **2008**, *73*, 1181–1191; c) M. Amorín, L. Castedo, J. R. Granja, *Chem. Eur. J.* **2008**, *14*, 2100–2111; d) T. Koga, M. Matsuoka, N. Higashi, *J. Am. Chem. Soc.* **2005**, *127*, 17596–17597; e) D. T. Bong, T. D. Clark, J. R. Granja, M. R. Ghadiri, *Angew. Chem.* **2001**, *113*, 1016–1041; *Angew. Chem. Int.*

Ed. **2001**, *40*, 988–1011; f) D. Ranganathan, *Acc. Chem. Res.* **2001**, *34*, 919–930.

[10] a) K. B. Joshi, S. Verma, *Angew. Chem.* **2008**, *120*, 2902–2905; *Angew. Chem. Int. Ed.* **2008**, *47*, 2860–2863; b) X. Yan, Y. Cui, Q. He, K. Wang, J. Li, W. Mu, B. Wang, Z. Ou-yang, *Chem. Eur. J.* **2008**, *14*, 5974–5980; c) A. Mahler, M. Reches, M. Rechter, S. Cohen, E. Gazit, *Adv. Mater.* **2006**, *18*, 1365–1370; d) Y.-B. Lim, E. Lee, M. Lee, *Angew. Chem.* **2007**, *119*, 9169–9172; *Angew. Chem. Int. Ed.* **2007**, *46*, 9011–9014; e) M. Reches, E. Gazit, *Nano Lett.* **2004**, *4*, 581–585; f) E. Gazit, *FASEB J.* **2002**, *16*, 77–83; g) S. Vauthey, S. Santoso, H. Gong, N. Watson, S. Zhang, *Proc. Natl. Acad. Sci. USA* **2002**, *99*, 5355–5360.

[11] a) I. Alfonso, M. Bolte, M. Bru, M. I. Burguete, S. V. Luis, *Chem. Eur. J.* **2008**, *14*, 8879–8891; b) I. Alfonso, M. Bolte, M. Bru, M. I. Burguete, S. V. Luis, J. Rubio, *J. Am. Chem. Soc.* **2008**, *130*, 6137–6144; c) M. Bru, I. Alfonso, M. I. Burguete, S. V. Luis, *Angew. Chem.* **2006**, *118*, 6301–6305; *Angew. Chem. Int. Ed.* **2006**, *45*, 6155–6159; d) M. Bru, I. Alfonso, M. I. Burguete, S. V. Luis, *Tetrahedron Lett.* **2005**, *46*, 7781–7785; e) J. Becerril, M. Bolte, M. I. Burguete, F. Galindo, E. García-España, S. V. Luis, J. F. Miravet, *J. Am. Chem. Soc.* **2003**, *125*, 6677–6686.

[12] a) J. Becerril, B. Escuder, J. F. Miravet, R. Gavara, S. V. Luis, *Eur. J. Org. Chem.* **2005**, 481–485; b) J. Becerril, M. I. Burguete, B. Escuder, F. Galindo, R. Gavara, J. F. Miravet, S. V. Luis, G. Peris, *Chem. Eur. J.* **2004**, *10*, 3879–3890; c) J. Becerril, M. I. Burguete, B. Escuder, S. V. Luis, J. F. Miravet, M. Querol, *Chem. Commun.* **2002**, 738–739.

[13] S. Ghosh, S. Verma, *Tetrahedron* **2008**, *64*, 6202–6208.

[14] a) C. Schmuck, T. Rehm, L. Geiger, M. Schäfer, *J. Org. Chem.* **2007**, *72*, 6162–6170; b) A. K. Das, S. Manna, M. G. B. Drew, S. Malik, A. K. Nandi, A. Banerjee, *Supramol. Chem.* **2006**, *18*, 645–655; c) C. Schmuck, W. Wienand, *J. Am. Chem. Soc.* **2003**, *125*, 452–459; d) K. Nakamura, H. Okubo, M. Yamaguchi, *Org. Lett.* **2001**, *3*, 1097–1099.

[15] a) Y. Tobe, N. Utsumi, K. Kawabata, A. Nagano, K. Adachi, S. Araki, M. Sonoda, K. Hirose, K. Naemura, *J. Am. Chem. Soc.* **2002**, *124*, 5350–5364; b) R. B. Martin, *Chem. Rev.* **1996**, *96*, 3043–3064.

[16] The suitable fitting to an isodesmic aggregation model nicely correlates with the very low gelation properties of this compound; for a recent discussion on this topic, see: A. R. Hirst, I. A. Coates, T. R. Boucheteau, J. F. Miravet, B. Escuder, V. Castelleto, I. W. Hamley, D. K. Smith, *J. Am. Chem. Soc.* **2008**, *130*, 9113–9121.

[17] a) A. Macchioni, G. Ciancaleoni, C. Zuccaccia, D. Zuccaccia, *Chem. Soc. Rev.* **2008**, *37*, 479–489; b) C. Schmuck, T. Rehm, F. Gröhn, K. Klein, F. Reinhold, *J. Am. Chem. Soc.* **2006**, *128*, 1430–1431; c) Y. Cohen, L. Avram, L. Frish, *Angew. Chem.* **2005**, *117*, 524–560; *Angew. Chem. Int. Ed.* **2005**, *44*, 520–554.

[18] Although the absolute changes in the chemical shifts of the aromatic protons are rather small, these changes are relevant when comparing the data between *para*/*meta* isomers measured in the same concentration range (0.41–41.0 mM); for example, the changes observed for *m*-**1b** ($|\Delta\delta| = 0.03$–0.05 ppm) are approximately fourfold the changes for **1b** ($|\Delta\delta| = \leq 0.01$ ppm); anyway, being aware of this small effect, we used the amide signals for the calculation of association constants because they display higher $\Delta\delta$ values.

[19] a) T. Haino, M. Tanaka, Y. Fukazawa, *Chem. Commun.* **2008**, 468–470; b) T. Itahara, K. Imaizumi, *J. Phys. Chem. B* **2007**, *111*, 2025–2032.

[20] a) S. R. Diegelmann, J. M. Gorham, J. D. Tovar, *J. Am. Chem. Soc.* **2008**, *130*, 13840–13841; b) X. Yan, Q. He, K. Wang, L. Duan, Y. Cui, J. Li, *Angew. Chem.* **2007**, *119*, 2483–2486; *Angew. Chem. Int. Ed.* **2007**, *46*, 2431–2434; c) J.-H. Ryu, H.-J. Kim, Z. Huang, E. Lee, M. Lee, *Angew. Chem.* **2006**, *118*, 5430–5433; *Angew. Chem. Int. Ed.* **2006**, *45*, 5304–5307.

[21] a) A. Ajayaghosh, R. Varghese, S. Mahesh, V. K. Praveen, *Angew. Chem.* **2006**, *118*, 7893–7896; *Angew. Chem. Int. Ed.* **2006**, *45*, 7729–7732; b) A. Mohanty, J. Dey, *Langmuir* **2004**, *20*, 8452–8459.

[22] a) E. Vass, M. Hollósi, F. Besson, R. Buchet, *Chem. Rev.* **2003**, *103*, 1917–1954; b) A. Menikh, M. T. Saleh, J. Gariepy, J. M. Boggs, *Biochemistry* **1997**, *36*, 15865–15872.

[23] S. H. Kim, D. Hartgerink, M. R. Ghadiri, *J. Am. Chem. Soc.* **1998**, *120*, 4417–4424.

[24] U. K. Slotta, S. Rammensee, S. Gorb, T. Scheibel, *Angew. Chem.* **2008**, *120*, 4668–4670; *Angew. Chem. Int. Ed.* **2008**, *47*, 4592–4594.

[25] In addition to the results from the theoretical calculations, the proposed shielding effect of amide groups by aromatic side chains is supported by the lower chemical shift of NH protons in *m*-**1b** relative to the shifts of *m*-**1a**, especially at very low concentration (Figure 5); for similar behavior in related compounds, see: a) I. Alfonso, M. I. Burguete, F. Galindo, S. V. Luis, L. Vigara, *J. Org. Chem.* **2007**, *72*, 7947–7956; b) I. Alfonso, M. I. Burguete, S. V. Luis, *J. Org. Chem.* **2006**, *71*, 2242–2250.

[26] S. Ghosh, S. Verma, *Chem. Eur. J.* **2008**, *14*, 1415–1419.

Received: August 6, 2009
Published online: December 8, 2009

